H^+-ion conductivity and ferroelectric properties of rubidium ammonium hydrogen sulphate

2001 J. Phys.: Condens. Matter 13 8509

(http://iopscience.iop.org/0953-8984/13/37/308)

INSTITUTE OF PHYSICS PUBLISHING JOURNAL OF PHYSICS: CONDENSED MATTER

J. Phys.: Condens. Matter **13** (2001) 8509–8518 PII: S0953-8984(01)21539-2

H^+-ion conductivity and ferroelectric properties of rubidium ammonium hydrogen sulphate

H Feki[1], **H Khemakhem**[2] **and Y Abid**[1]

[1] Laboratoire de Physique Moléculaire et Cristalline, Faculté des Sciences de Sfax, 3018, BP 802, Sfax, Tunisia[3]
[2] Laboratoire des Matériaux Ferroélectriques et Conducteurs Ioniques, Faculté des Sciences de Sfax, Département de Physique, Sfax, Tunisia

E-mail: younes.abid@fss.rnu.tn (Y Abid) and hamadi.khemakhem@fss.rnu.tn (H Khemakhem)

Received 12 February 2001, in final form 9 May 2001
Published 30 August 2001
Online at stacks.iop.org/JPhysCM/13/8509

Abstract

Electric and dielectric measurements have been used to study the superionic conductivity and the ferroelectricity respectively in $Rb_{0.8}(NH_4)_{0.2}HSO_4$ single crystal. This material presents a high level of conductivity at high temperature. Activation energies were determined from the temperature dependence of the alternating-current conductivity in the regions 440–560 K and beyond 560 K; they are respectively 0.15 and 0.10 eV. The dielectric measurements show an intense anomaly at 285 K indicating a ferroelectric–paraelectric phase transition. This phase transition is accompanied by a significant dispersion of the real part of the dielectric constant in the frequency region investigated, in accordance with the high level of conductivity of this material.

1. Introduction

Substitution of ammonium (NH_4) for caesium, rubidium or potassium in sulphates modifies the ionic conductivity and can be the cause of the appearance of a polar phase at low temperature and a superionic protonic phase at high temperature [1–3]. This behaviour was interpreted in our last work [4] as due to the fact that the NH_4 (ammonium) group exhibits static and dynamic orientational disorder; this has been studied in other work [5]. The ferroelectric characteristics of these materials can be modified by this substitution [1, 2, 6, 7].

In our last work, we studied these properties for the composition with $x = 0.4$ of the solid-solution series $Rb_{1-x}(NH_4)_xHSO_4$ [4].

In the present work, we propose to study the modification of these properties in $Rb_{0.8}(NH_4)_{0.2}HSO_4$ single crystal, motivated by their advantageous properties on one hand and their non-trivial character on the other hand. This family of materials, which combine

[3] Fax: 216 4274437.

the properties of ferroelectricity and a superconducting protonic phase, have been subject to intensive research in recent years [8–11] due to their important applications. In fact, these materials can be used in various electrochemical devices such as batteries, fuel cells, electrochemical sensors and electrochemical reactors [8, 9]. Our study was carried out using dielectric and electric measurements. The relaxation studies were performed using the complex-modulus M^*-formalism.

2. Experimental procedure

$Rb_{0.8}(NH_4)_{0.2}HSO_4$ single crystal was obtained by slow evaporation at 300 K of H_2SO_4, Rb_2SO_4 and $(NH_4)_2SO_4$ aqueous solutions. The rubidium ammonium sulphate contents were checked by chemical analysis and the sample composition was confirmed. The method used was described in our earlier works [1, 2]. a.c. impedance measurements were made over the frequency range 5–1.3 $\times$ 10^7 Hz using an HP 4192A analyser over the temperature range 250–550 K. The complex permittivity $\varepsilon^*(\omega) = \varepsilon'_r - i\varepsilon''_r$ was measured over the frequency and temperature ranges 10^2–2 $\times$ 10^5 Hz and 150–450 K respectively using a Wayne–Kerr capacitance bridge (model 6425). The single crystal was electroded on the two faces perpendicular to the polar axis.

3. Ionic conductivity

Before the measurements, the samples were heated for 4 h at 150 °C to eliminate as much as possible the water deposited on the crystal faces. The sample was put into a quartz tube shielded by a Faraday cage. The measurements were carried out in air at 20 or 10 °C intervals. At each measurement temperature T, the sample was maintained at $T \pm 0.5$ °C for 30 min before we collected the data. Figure 1 presents for several temperatures the variation of the imaginary part of the impedance versus frequency. From this evolution, we observe that the peaks of these curves, which indicate the relaxation frequency, shift to higher frequencies and decrease in intensity when temperature increases. This behaviour shows that the proton became more free at high temperature.

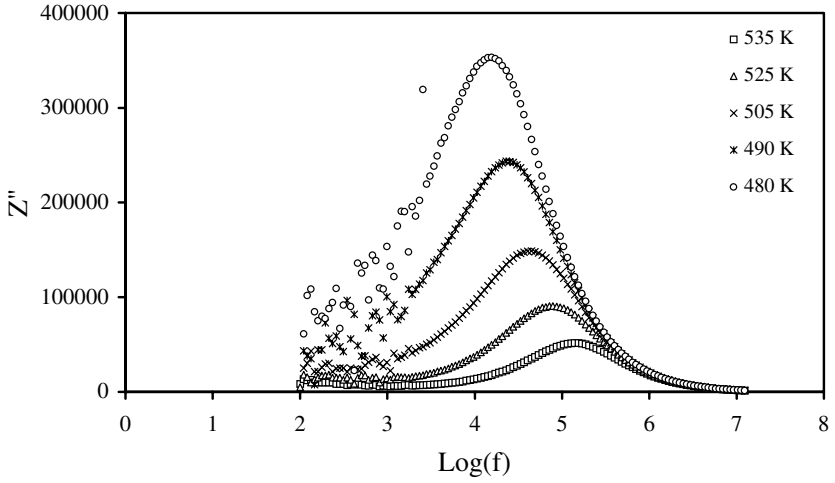

Figure 1. The frequency evolution of the imaginary part of Z^* for the temperatures 480, 490, 505, 525 and 535 K over the frequency range 10^2–10^7 Hz.

Some typical Cole–Cole plots are shown in figure 2. The results in fact lead to a circular-like arc skewed in the low-frequency region because of the resistance limitations of our instruments. The temperature dependence of the ionic conductivity was determined for the single crystal $Rb_{0.8}(NH_4)_{0.2}HSO_4$. Figure 3 shows the evolution of the conductivity versus inverse temperature, $\log_{10}(\sigma T) = f(1000/T)$, for this material. A substantial jump of the conductivity was observed at 450 K.

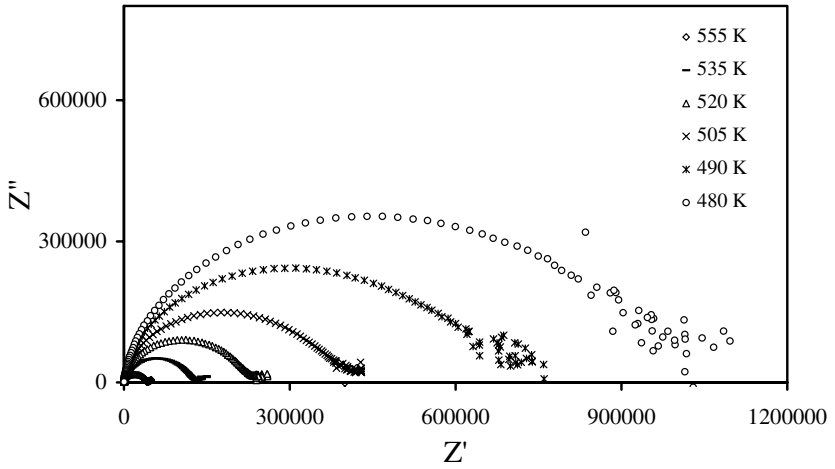

Figure 2. Complex-plane plots of the impedance (Z'', Z') of $Rb_{0.8}(NH_4)_{0.2}HSO_4$ at various temperatures.

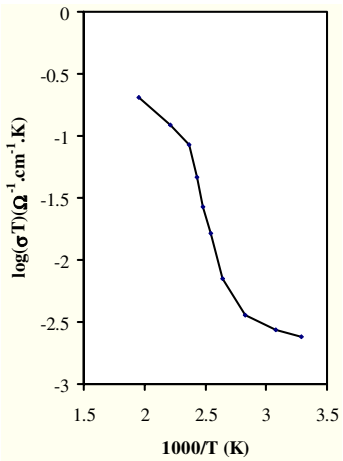

Figure 3. The temperature dependence of $\log(\sigma T)$ for $Rb_{0.8}(NH_4)_{0.2}HSO_4$ over the temperature range 300–550 K.

This behaviour indicates a superionic–protonic phase transition in this material. This transition presents a deviation to higher temperatures compared to that observed in our earlier studies performed on the $x = 0.4$ composition (table 1). However, the values of the conductivity present a significant evolution in the present material for low and high temperatures. This modification could be due to the fact that the small amount of ammonium

Table 1. Electrical characteristics of $Rb_{1-x}(NH_4)_xHSO_4$ ($x = 0.4$ and 0.2) at room temperature and in the superionic phase.

	T_C	T_{SCP}	σ_{SCP} (Ω^{-1} cm^{-1})	$\sigma_{(amb)}$ (Ω^{-1} cm^{-1})
$Rb_{0.6}(NH_4)_{0.4}HSO_4$	290	415	7.6×10^{-7}–2.2×10^{-6}	1.8×10^{-7}
$Rb_{0.8}(NH_4)_{0.2}HSO_4$	285	450	2.3×10^{-4}–4×10^{-4}	7×10^{-6}–9×10^{-6}

introduces more disorder than a great amount, because the small amount can be considered as a perturbation in the lattice. At low temperature the conductivity does not obey the Arrhenius law. In the two regions 440–560 K and beyond 560 K, the conductivity obeys the Arrhenius law and the activation energies are $\Delta E_{\sigma 1} = 0.15$ eV and $\Delta E_{\sigma 2} = 0.10$ eV respectively. However, in the low-temperature region the conductivity could be due to the competition of some conductivity mechanisms such as the tunnelling mechanism. These mechanisms could be considered to be electrode-related phenomena. On the basis of the above, we can consider the experimental data in this region to represent a circular arc and not to obey the Arrhenius law.

The complex-modulus formalism, $M^* = 1/\varepsilon^* = i\omega C_0 Z^*$ where $i = \sqrt{-1}$, $\omega = 2\pi f$ is the angular frequency and C_0 is the vacuum capacitance of the cell, has been adopted to determine the conductivity relaxation times. This formalism automatically excludes electrode polarization and other interfacial effects in solid electrolytes [12]. Plots of the real part of $M^*(\log M')$ versus $\log f$ are given in figure 4 for various temperatures. At high frequency M' reaches a constant value M'_∞ ($M'_\infty = 1/\varepsilon'_\infty$) and at low frequencies it approaches zero. This behaviour shows that electrode polarization phenomena make a negligible contribution to M^*; thus we can ignore them when we analyse the electric data using this formalism [13].

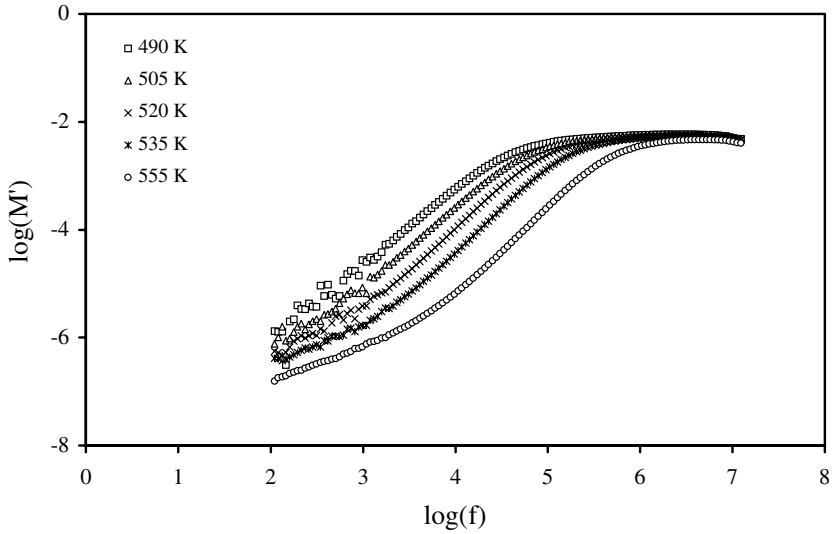

Figure 4. Plots of $\log M'$ versus $\log(f)$ for $Rb_{0.8}(NH_4)_{0.2}HSO_4$ at various temperatures.

Plots of M''/M''_{max}, the normalized imaginary part of M^*, versus $\log f$ at various temperatures are given in figure 5. The frequency f_p relative to M''_{max} ($f_p = 1/2\pi\tau_\sigma$) is governed by the condition $\omega\tau_\sigma = 1$, where τ_σ is the most probable ion relaxation time; its value is 5×10^{-6} s at 440 K and becomes 2.5×10^{-7} s at 500 K. This decrease is attributed to the fact that the proton presents a transition from displacements over small distances at low

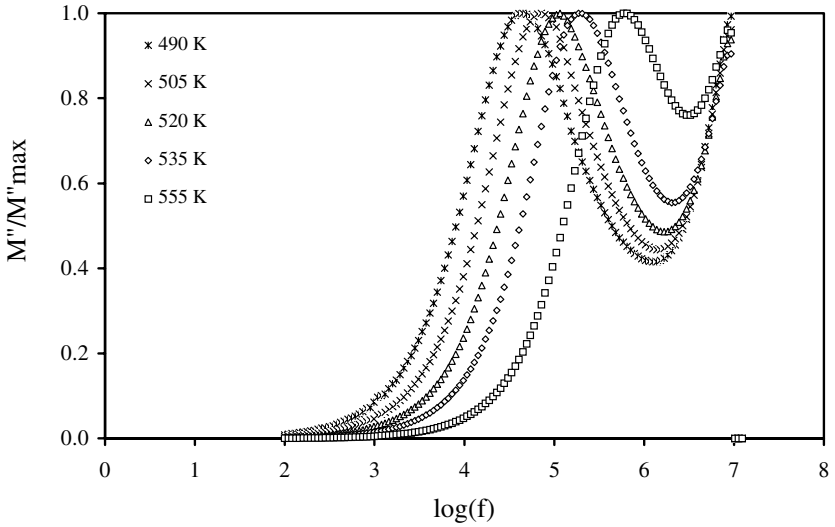

Figure 5. Plots of the normalized modulus (M''/M''_{max}) versus $\log(f)$ for $Rb_{0.8}(NH_4)_{0.2}HSO_4$ at various temperatures over the frequency range 10^2–10^7 Hz.

temperature to displacements over long ranges at high temperature. These latter displacements are of the order of magnitude of the displacements involved in proton relaxation. f_p increases with increasing temperature and the temperature dependence of f_p is of Arrhenius type: $f_p = f_{p0}\exp(-\Delta E_p/kT)$, where ΔE_p is the energy deduced from the modulus spectra (figure 6). $\log(f_p)$ versus $1000/T$ shows an anomaly at 470 K, which can be attributed to the

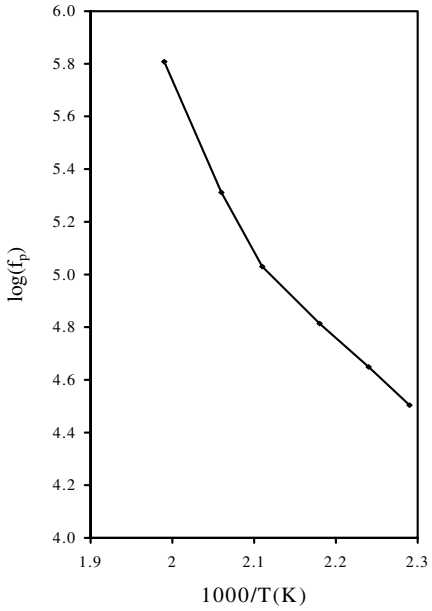

Figure 6. The thermal evolution of $\log(f_p)$, where f_p is the M''_{max}-peak for $Rb_{0.8}(NH_4)_{0.2}HSO_4$.

fact that the protons go from a non-conductor state to a superconductor state. The energies for the conductor and superconductor states are $\Delta E_{p1} = 0.24$ eV and $\Delta E_{p2} = 0.51$ eV respectively.

The superimposed plots of $\log(M'')$ and of $\log(M')$ given in figure 7 were obtained by scaling each frequency by the frequency of the maximum in M''. The near-perfect overlap of the data for different temperatures, superimposed on the simple 'master' curve, are in agreement with the assertion that all dynamic processes occurring at different frequencies exhibit the same thermal activation energy. However, we cannot attribute the non-exponential relaxation to the distribution of activation energies [14].

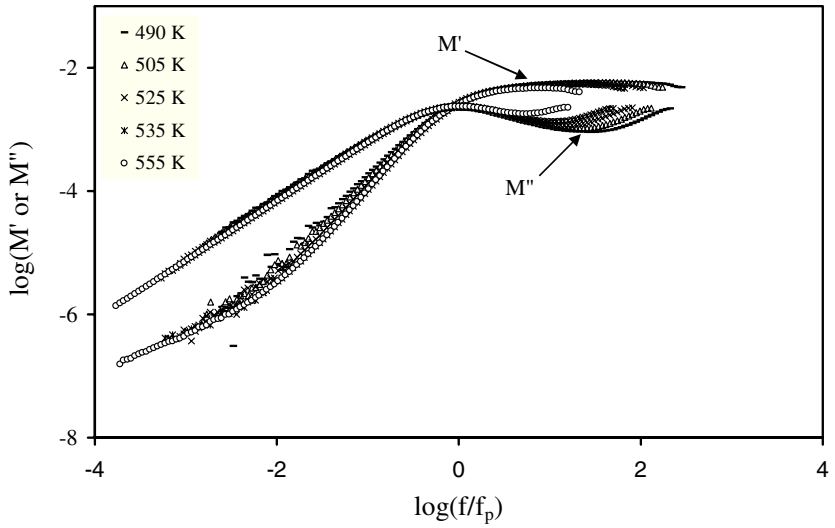

Figure 7. A master plot of both the real and the imaginary parts of the electrical modulus for $Rb_{0.8}(NH_4)_{0.2}HSO_4$.

4. Dielectric measurements

The dielectric measurements were performed on $Rb_{0.8}(NH_4)_{0.2}HSO_4$ crystal with the electric field along the *c*-axis which represents the polar axis. The thermal evolution of ε'_r versus temperature (figure 8) shows the familiar characteristics of a second-order phase transition. This transition was interpreted as of ferroelectric–paraelectric type. This interpretation was based on studies performed on the two materials $RbHSO_4$ and NH_4HSO_4 [6, 7]. ε'_r presents a significant decrease with increasing frequency; this behaviour can be interpreted as a dispersion in such materials which could be due to charge carriers present in the material and to the high mobility of the atoms and especially H^+. This behaviour was observed in our earlier works [15, 16] and in those cases the dielectric constant presented two contributions which represent the lattice and the conductivity relaxation, or carrier response, respectively:

$$\varepsilon'_{r(meas)} = \varepsilon'_{r(latt)} + \varepsilon'_{r(carr)}.$$

Here, $\varepsilon'_{r(latt)}$ represents the lattice response due to permanent dipole orientations or other motions which do not involve long-range displacements of mobile charge carriers, while $\varepsilon'_{r(carr)}$ represents the conductivity relaxation, or carrier response, associated with long-range migration.

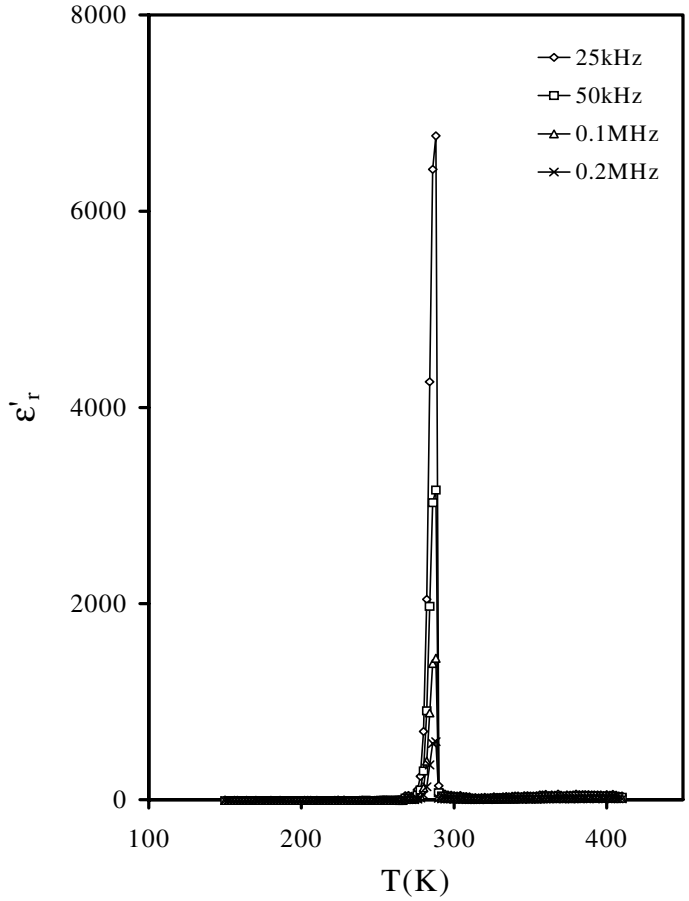

Figure 8. The thermal evolution of the dielectric constant ε_r' over the frequency range $10–2\times10^5$ Hz.

The measured complex permittivity can be decomposed into real and imaginary parts:

$$\varepsilon_r'(w)_{(meas)} = \varepsilon_\infty + \frac{(\varepsilon_s - \varepsilon_\infty)[1 + (w/w_1)^m \cos(m\pi/2)]}{1 + 2(w/w_1)^m \cos(m\pi/2) + (w/w_1)} + \frac{\sigma_0}{\varepsilon_0 w}\left(\frac{w}{w_2}\right)^n \sin\left(\frac{n\pi}{2}\right)$$

and

$$\varepsilon_r''(w)_{(meas)} = \varepsilon_\infty + \frac{(\varepsilon_s - \varepsilon_\infty)[1 + (w/w_1)^m \sin(m\pi/2)]}{1 + 2(w/w_1)^m \cos(m\pi/2) + (w/w_1)} + \frac{\sigma_0}{\varepsilon_0 w}\left(\frac{w}{w_2}\right)^n \cos\left(\frac{n\pi}{2}\right).$$

Also the complex conductivity permittivity can be decomposed into real and imaginary parts:

$$\varepsilon_r'(w)_{(carr)} = \frac{\sigma_0}{\varepsilon_0 w}\left(\frac{w}{w_2}\right)^n \sin\left(\frac{n\pi}{2}\right)$$

and

$$\varepsilon_r''(w)_{(carr)} = \frac{\sigma_0}{\varepsilon_0 w}\left[1 + \left(\frac{w}{w_2}\right)^n \cos\left(\frac{n\pi}{2}\right)\right].$$

Here, w_1 and m characterize the dielectric relaxation (lattice response), while w_2 and n characterize the conductivity relaxation (carrier response). The parameters σ_0, n and w_2

can be determined from the curves for $Z'' = f(Z')$ and $Z'' = f(\log f)$. Also,

$$\varepsilon'_r(w)_{(latt)} = \varepsilon'_r(w)_{(meas)} - \varepsilon'_r(w)_{(carr)}$$

$$\varepsilon''_r(w)_{(latt)} = \varepsilon''_r(w)_{(meas)} - \varepsilon''_r(w)_{(carr)}.$$

As observed in the case of the composition with $x = 0.4$ from the solid-solution series $Rb_{1-x}(NH_4)_xHSO_4$ [7], the paraelectric–ferroelectric phase transition temperature does not change with increasing frequency, which suggests that no dielectric relaxation is present in this frequency range. However, the conductivity relaxation could be observed at lower frequencies.

If we compare the Curie temperature for this composition with that obtained for other compositions, we note that the temperature increases with ammonium content increasing from $x = 0$, presents a maximum at $x = 0.4$, then decreases as the content decreases to $x = 1$ [5, 7, 14]. We can interpret this behaviour as follows. The covalency of the bonds decreases when the content of the disordering group (NH_4^+) is in the vicinity of 50% and in that case the ferroelectric temperature T_c is maximum because this temperature marks the disappearance of the spontaneous polarization in this material.

Figure 9 presents the evolution of $1/\varepsilon'_r$ versus temperature for this composition at $f = 25$ kHz. We observe that $1/\varepsilon'_r$ varies linearly in the ferroelectric phase and the ε'_r-variation obeys a Curie–Weiss law:

$$\varepsilon'_r = \frac{c}{T - T_c}.$$

However, in the paraelectric phase, ε'_r does not obey the Curie–Weiss law. This deviation from linear behaviour could be due to the conduction phenomenon, which became significant at high temperature.

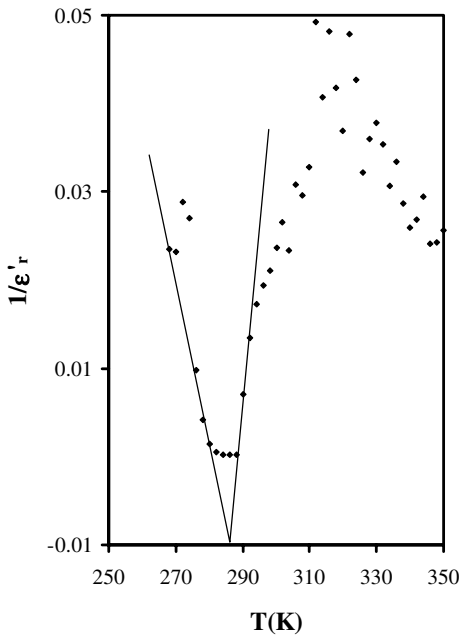

Figure 9. The thermal evolution of $1/\varepsilon'_r$ at the frequency 25×10^3 Hz.

Because of the small sizes of the crystals on one hand and the significant conductivity on the other hand, measuring the spontaneous polarization and piezoelectric coefficients became very difficult.

Figure 10 shows the temperature dependence of the dissipation factor $\tan\delta$ at different frequencies. From this evolution we can see that this dispersion of the dissipation factor has characteristics common to crystals of the KDP family. $\tan\delta$ takes small values at low temperatures; then it increases, presenting a peak at T_c indicating the ferroelectric–paraelectric phase transition. The large dispersion of the values of $\tan\delta$ with variation of the frequency at T_c is in accord with the significant conductivity in this material. Beyond $T = 400$ K, $\tan\delta$ increases, marking the transition from a conductor to a superconductor state [17].

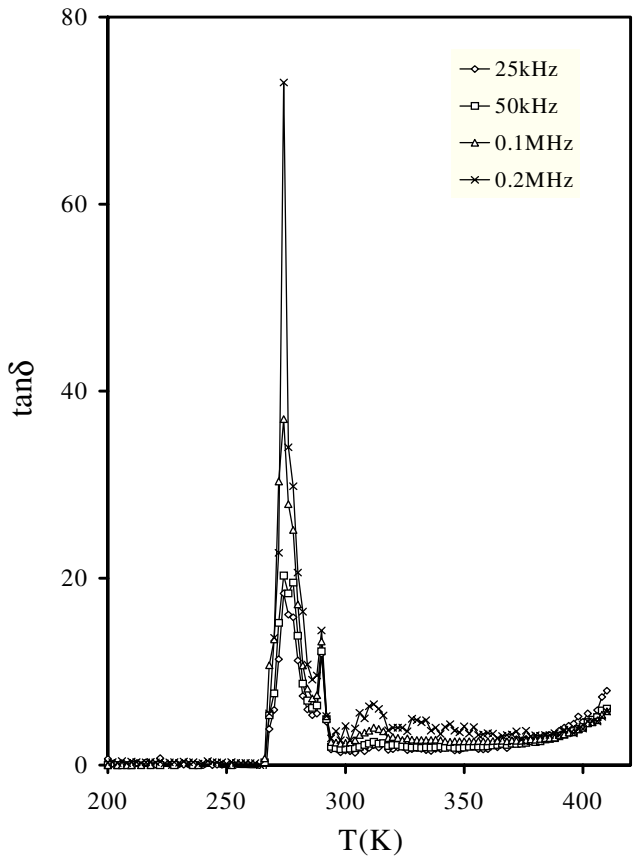

Figure 10. The temperature evolution of $\tan\delta$ for the frequencies 25, 50, 100 and 200 kHz.

5. Conclusions

The evolutions of the dielectric constant and the conductivity versus temperature for the compound $Rb_{0.8}(NH_4)_{0.2}HSO_4$ show that this material presents a ferroelectric–paraelectric phase transition at 285 K, a substantial dispersion and a superionic phase transition at 450 K. This superionic conductivity is due to H^+ mobility. From these measurements, we deduce that the dielectric permittivity presents—as for the case of the composition with $x = 0.4$ of the same solid-solution series—two contributions; one represents the lattice response and the other represents the charge-carrier response. These studies will be complemented by spontaneous polarization measurements, which are under way.

The superionic phase presents a modification in level of conductivity compared to that of the composition with $x = 0.4$. This modification was interpreted as due to the small amount of ammonium; ammonium induces a larger dynamic orientational disorder when it is present in small amounts than when its content is of the same order of magnitude as that of the rubidium.

References

[1] Khemakhem H, Mhiri T, Fakhfakh Z and Daoud A 1996 *Phase Transitions* **56** 193
[2] Khemakhem H, Mhiri T, Fakhfakh Z and Daoud A 1994 *Adv. Mater. Res.* **1+2** 299
[3] Mhiri T and Colomban Ph 1989 *Solid State Ion.* **35** 99
[4] Khemakhem H, Mhiri T and Daoud A 1999 *Solid State Ion.* **117** 337
[5] Perry C H and Lowdes R P 1969 *J. Chem. Phys.* **51** 3648
[6] Pepinsky R, Vedam K, Hoshino S and Okaya Y 1958 *Phys. Rev.* **111** 1508
[7] Pepinsky R and Vedam K 1960 *Phys. Rev.* **117** 1502
[8] Vargas R A, Torijans E, Diosa J E and Mellanders B E 1999 *Solid State Ion.* **125** 187
[9] Solinsek J, Karayanri M and Papavassiliou G 1999 *Solid State Ion.* **125** 159
[10] Schmidt V H, Lanceros-Mendez S, Meschia S C and Pinto N J 1999 *Solid State Ion.* **125** 147
[11] Belushkin A V, Adams M A, Hull S and Shuvalov L A 1995 *Solid State Ion.* **77** 91
[12] Almand D P and West A R 1983 *Solid State Ion.* **11** 57
[13] Howell F S, Bose R A, Macedo P B and Moynihan C T 1974 *J. Phys. Chem.* **78** 639
[14] Patel H K and Martin S W 1992 *Phys. Rev.* B **45** 10 292
[15] Khemakhem H, Mnif M, Ravez J and Daoud A 1999 *J. Phys. Soc. Japan* **68** 41
[16] Khemakhem H 1999 *Ferroelectrics* **234** 47
[17] Bierlein J D and Vanherzeele H 1989 *J. Opt. Soc. Am.* **6** 622